Iraqi J. Laser, issue 1, vol., 22, pp. 51-58 (2023)

IRAQI JOURNAL OF LASER

Performance Study of Polarization Beam Splitters Based on Horizontal Slot Waveguide Operating at 700nm Wavelength

Salwa Marwan Salih, Shelan Khasro Tawfeeq*
Institute of Laser for Postgraduate Studies, University of Baghdad, 10070 Baghdad, Iraq
Corresponding author: salwa.saleh1001@ilps.uobaghdad.edu.iq

(Received 16/04/2023; accepted 25/05/2023)

Abstract: Polarization beam splitter (PBS) integrated waveguides are the key components in the receiver of quantum key distribution (QKD) systems. Their function is to analyze the polarization of polarized light and separate the transverse-electric (TE) and transverse-magnetic (TM) polarizations into different waveguides. In this paper, a performance study of polarization beam splitters based on horizontal slot waveguide has been investigated for a wavelength of 700 nm. PBS based on horizontal slot waveguide structure shows a polarization extinction ratio for quasi-TE and quasi-TM modes larger than 15 dB with insertion loss below 1 dB and a bandwidth of ~7 nm. Also, the fabrication tolerance of the structure is analyzed.

Keywords: Polarization beam splitter, coupling mode, extinction ratio

1. Introduction

Silicon photonics has attracted attention for building high-density photonic integrated circuits due to its compatibility with mature complementary metal-oxide-semiconductor (CMOS) technology [1]. The polarization dependence characteristics can be caused by high index contrast and asymmetric structure, therefore a polarization diversity such as a polarization beam splitter is required [2].

The function of PBS is to separate the transverse-electric (TE) and transverse-magnetic (TM) polarizations of polarized light into different waveguides. The performance of PBS depends on important parameters which are polarization extinction ratio (PER), insertion loss (IL), operating bandwidth, and fabrication tolerance [3].

Different structures of PBSs have been demonstrated such as multimode interferometers (MMIs) [4], Mach-Zehnder interferometers (MZIs) [5], gratings [6], hybrid plasmonic waveguides [7], directional couplers including symmetric and asymmetric waveguides [8] and slot waveguides [9].

MMI and MZI PBSs induce large insertion loss and footprint, while grating-based structures can achieve a small footprint but with large scattering losses [8],[10]. Using hybrid plasmonic waveguides can shorten the structure length but this type of waveguide suffers from high losses due to metal absorption [11]. PBSs based on symmetric directional couplers are preferred due to their simple design and good performance [12]. While asymmetric directional coupler (ADC) structures require two or more different waveguides to increase the refractive index contrast and attain PBS with a high extinction

ratio, fabrication tolerance, and small footprint [13].

Slot waveguides have been employed recently due to their strong field confinement in the low refractive index nanoscale slot region. A slotted waveguide consists of a layer of low refractive index material sandwiched between two layers of high refractive index materials so that light is mostly confined in the slot region. They can be classified into two categories; horizontally oriented slots within which transverse magnetic (TM) is confined and vertically oriented slots for transverse electric (TE) polarization confinement [14].

Various schemes using slot waveguides have been proposed such as half-etch horizontal slot waveguides [15], PBS assisted by subwavelength grating in triple waveguide directional coupler [16], asymmetric silicon slot-waveguide-assisted [17], and horizontal nanoplasmonic slot waveguides [18].

Recently, integrated photonic technology has been emerged in QKD research, with a series of photonic chips designed for QKD applications [19]. The stability of the QKD system is improved and its cost may be significantly reduced by integrating the optical components of the QKD system, including single-photon sources, that operates in the visible region on a single photonic chip [20],[21].

Free-space QKD generally uses short wavelength due to low atmospheric absorption and efficient operation of Si single photon detector [22]. Thus, different types of PBSs have been developed at visible wavelength [23],[24].

In this paper, we will investigate the operation of PBS based on a dual-channel directional coupler horizontal slot waveguide (DC-HSW) at a wavelength of 700 nm. The integrated PBS in the receiver chip is required to analyze the polarized light sent by single-photon sources for QKD systems based on the BB84 protocol operating at 700 nm. The devices were numerically simulated using COMSOL Multiphysics 6.0 by 2D and 3D frameworks. The device is patterned on silicon on an insulator substrate with air as an upper cladding.

This paper is organized as follows: Section 2 describes the design of the PBS based on dual-channel (DC-HSW), the optical properties, and its wavelength dependence. Section 3 is related to fabrication tolerance for PBS based on dual-channel (DC-HSW). Finally, the conclusions are presented in Section 4.

2. Design of the PBS based on dual-channel (DC-HSW)

Figure 1(a) shows the schematic structure of PBS based on dual-channel (DC-HSW). The structure consists of a slot layer of hydrogen silsesquioxane (HSQ) sandwiched between two layers of gallium phosphide (GaP). The refractive indices of air, HSQ, and GaP are (1, 1.41, and 3.2543) respectively. The slot layer supports the optical signal to be guided at a wavelength of 700 nm.

In the 2D framework, the dimensions of a single horizontal slot waveguide (HSW) were found by fixing the slot height, $h_{slot} = 30$ nm, and tuning the width and height of GaP layers w and h_w respectively. The optimal dimensions for w and h_w are 130 nm and 200 nm respectively.

Figures 1(b) and 1(c) show the transverse mode profile for quasi-TE and quasi-TM modes for a single HSW. The quasi-TM mode is strongly confined in the slot region due to discontinuity between high and low refractive index regions.

When the light propagates in such a dual-channel DC, the guiding behavior of the total device can be viewed as the summation of waves propagating in even and odd modes with effective indices n_e and n_o respectively, as shown in Figures 2(a)-2(d). These modes can be observed due to the differences in the field continuity at boundaries between the core and the cladding. The evolution of the effective index of each corresponding waveguide mode as a function of the waveguide width (w_g) is shown in Figure 2 (e).

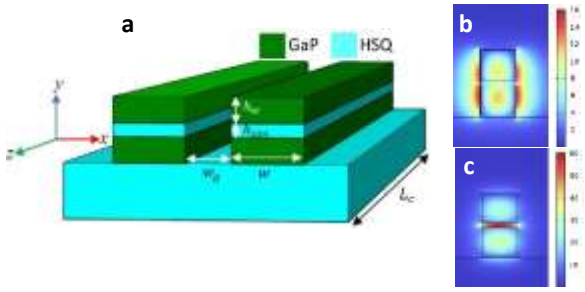

Fig. 1: (a) Schematic of a PBS based on dual-channel (DC-HSW). (b) Transverse field distribution of quasi-TE mode and (c) quasi-TM mode in single HSW

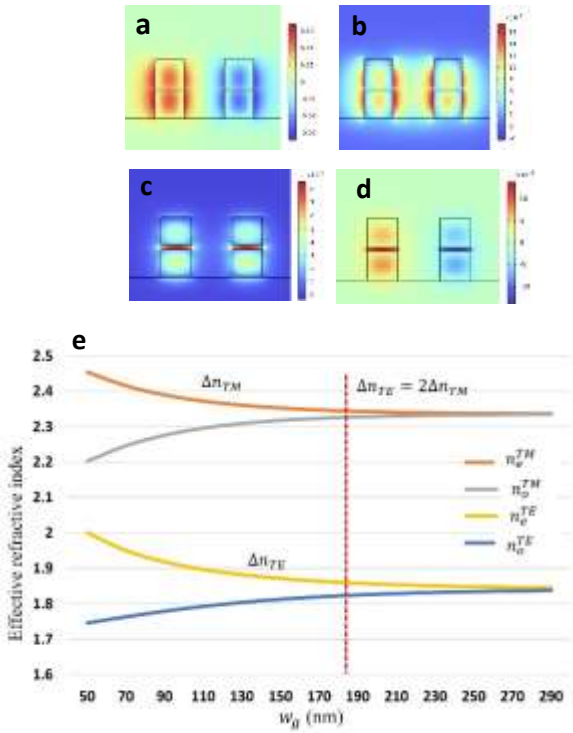

Fig. 2: Transverse field distribution of quasi-TE and quasi-TM modes in dual-channel waveguides. (a) even quasi-TE mode (b) odd quasi-TE mode (c) even quasi-TM mode (d) odd quasi-TM mode and (e) the effective indices of even and odd of quasi-TM (n_e^{TM}, n_o^{TM}) and even and odd of quasi-TE (n_e^{TE}, n_o^{TE}) as a function of the gap width (w_g)

As it appears, when w_g decreases, the effective index difference between even and odd modes ($\Delta n = |n_e - n_o|$) increases because of the coupling between the propagating optical signals in both waveguides. Meanwhile, when w_g increases, the n_e and n_o modes converge to the effective index of individual HSW. In this case, the dual channels act as independent horizontal slot waveguides.

Following the supermode solution method [25],[26], the coupling length (L_c) required to transfer the power completely from the input to adjacent waveguides in a dual-channel DC is related to the difference between the effective indices of n_e and n_o for each quasi-TE and quasi-TM mode.

$$L_c = \frac{\pi}{k_0(n_e - n_o)} = \frac{\pi}{k_0 \Delta n} \qquad (1)$$

Where $k_0 = \frac{2\pi}{\lambda_0}$ is the propagation constant in free space at the operating wavelength λ_0.

As the width of GaP must satisfy ($w < 2h_w + h_{slot}$), the quasi-TM mode has strong confinement in the slot region while the quasi-TE mode has tails in the waveguide spacing region. As a result, the effective indices of quasi-TE mode may vary significantly as waveguide width increases.

According to the differences mentioned, the ratio of coupling lengths of the quasi-TE mode (L_c^{TE}) and quasi-TM mode (L_c^{TM}) can be tuned to different values of aspect ratios ($\frac{w}{h_w}$) as a function of the w_g as shown in Figure (3).

To simplify the design, h_{slot} was tuned to 30 nm for strong confinement, which will be discussed in section 3. The GaP layers with different aspect ratios, where for each value of $w = 120,130,$ and 140 nm; $h_w = 180, 190, 200,$ and 210 nm, were considered to manipulate the birefringence of the horizontal slot structure and the coupling effect based on Equation (1) between the adjacent waveguides.

Based on Figure (3), when w_g is more than120 nm, the effective index difference of the quasi-TE mode ($\Delta n_{TE} = n_e^{TE} - n_o^{TE}$) is larger than that of the quasi-TM mode ($\Delta n_{TM} = n_e^{TM} - n_o^{TM}$). By adjusting w_g, PBS with efficient polarization splitting can be achieved. Based on Equation (1), when $\Delta n_{TE} = 2\Delta n_{TM}$, the coupling length ratio is ($\frac{L_c^{TE}}{L_c^{TM}} = 0.5$). The incident light can be efficiently separated into two orthogonally polarized modes propagating in separate output ports. According to Figures (2) and (3), the

optimum dimensions of PBS were tuned using an optimization tool and illustrated in Table 1.

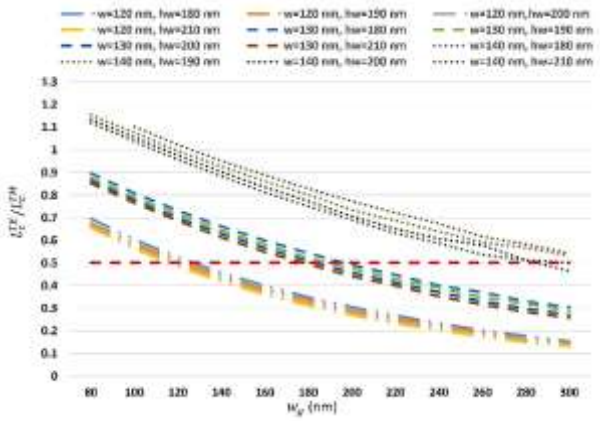

Fig. 3: Coupling length ratio of quasi-TE and quasi-TM modes as a function of the gap width (w_g) at different aspect ratios ($\frac{w}{h_w}$)

The Optimization tool is based on the formula of a general single-objective minimization problem. The goal of the optimization problem is to find the value of the control variables that minimizes (or maximizes) the objective function while considering a number of constraints. One of the optimization methods is the Monte Carlo solver, which samples points randomly within a uniform distribution by a user-specified box. The solver is effective for gathering statistical data for design variations by analyzing the range of values the objective function takes. This method is not stuck in local minima, unlike the other optimization methods implemented in COMSOL Multiphysics. It always analyzes the whole search space specified by the parameter boundaries.

The propagation of light for quasi-TE and quasi-TM modes is shown in Figure (4). It can be observed that quasi-TM mode is completely transferred to the cross port while quasi-TE mode bounced between the adjacent waveguides and is coupled out to the bar port.

Table (1): Dimensions of PBS based o dual-channel (DC-HSW)

Substrate width (μm)	Substrate height (μm)	w(nm)	h_w (nm)	h_{slot} (nm)	w_g (nm)	L_c (μm)
1.5	1	130	200	30	182	19

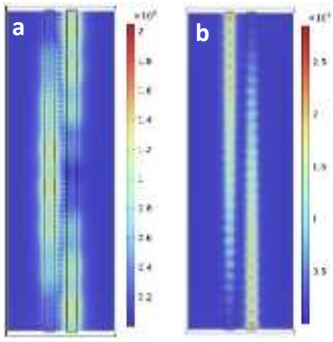

Fig. 4: Light propagation for (a) quasi-TE and (b) quasi-TM modes between the adjacent waveguides of PBS based on dual-channel DC-HSW

The wavelength dependence for quasi-TE mode and quasi-TM mode at bar and cross ports of PBS was investigated respectively, as shown in Figure (5). The polarization extinction ratio (PER) and insertion loss (IL) are the keys to the figure of merit for PBS and are defined as:

$$PER_{TE} = 10\ \log\frac{P_{bar}^{TE}}{P_{bar}^{TM}} \quad (2)$$

$$PER_{TM} = 10\ \log\frac{P_{cross}^{TM}}{P_{cross}^{TE}} \quad (3)$$

$$IL_{TE} = -10\log\frac{P_{bar}^{TE}}{P_{input}} \quad (4)$$

$$IL_{TM} = -10\log\frac{P_{cross}^{TM}}{P_{input}} \quad (5)$$

From Figure (6), it can be noticed that at the operating wavelength of 700 nm PERs are 20.49 dB and 17.36 dB for quasi-TE and quasi-TM modes, respectively. The bandwidths for IL $<$ 1dB and ER $>$ 15 dB are 6 nm and 7 nm for quasi-TE and quasi-TM modes respectively.

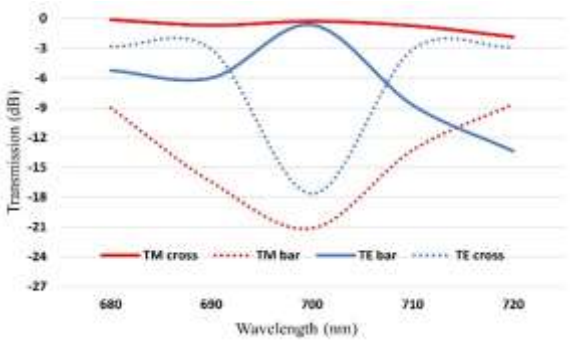

Fig. 5: Transmission spectrum for quasi-TE and quasi-TM modes for PBS based on dual-channel DC-HSW

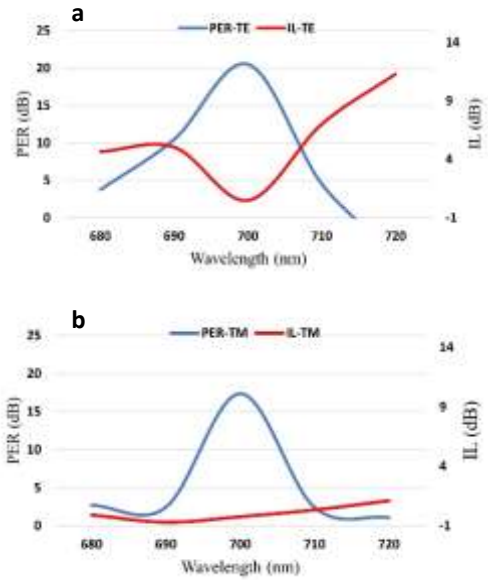

Fig. 6: Polarization extinction ratio and insertion loss for (a) quasi-TE and (b) quasi-TM modes for PBS based on dual-channel DC-HSW

The deviation in L_c shown in Figure (7) was investigated as a parametric study. The deviation is within 2 µm (from 18 to 20 µm) for keeping the transmission higher than -3 dB. If the deviation range in L_c is larger than 2 µm, the transmission behavior for quasi-TE mode is varied as the condition in Equation (1) is not fulfilled.

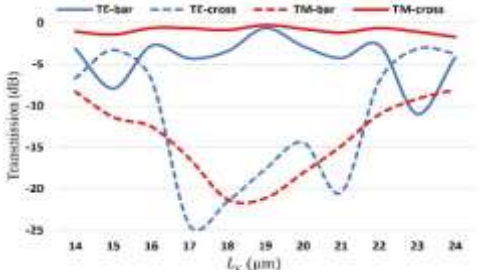

Fig. 7: Transmission spectrum of quasi-TE and quasi-TM modes as a function of coupling length (L_c) for PBS based on dual-channel DC-HSW

3. Fabrication tolerance

A directional coupler based on PBS is usually sensitive to dimension deviation due to fabrication tolerance. Optical lithography and etching are two processes that can be used in the fabrication of PBS based on dual-channel (HSW-DC). These two processes cause deviations in the dimensions of the designed structures.

The fabrication tolerances of w and h_{slot} of PBS based on dual-channel (DC-HSW) are shown in Figures 8(a) and 8(b). It can be observed that the tolerance for quasi-TE mode is more critical compared to quasi-TM mode. The deviations in w and h_{slot} are limited to a very small range of 2 nm.This is because the mode-field distribution and consequently the effective indices for quasi-TE and quasi-TM modes require transverse geometry.

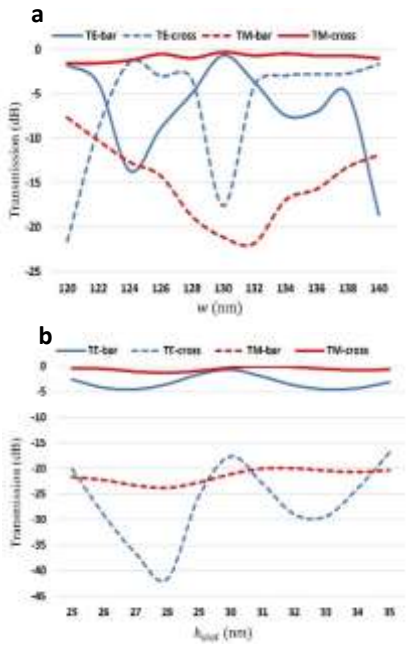

Fig. 8: Transmission spectrum of quasi-TE and quasi-TM modes as a function of (a) width of the waveguide (w), and (b) slot thickness (h_{slot}) for PBS based on dual-channel DC-HSW

Table 2 lists a comparison between the designed structure and other structures mentioned in literature.

4. Conclusion

The performances of PBS based on dual-channel (DC-HSW) has been investigated for a wavelength of 700 nm. With appropriate waveguide dimensions, the structural birefringence in the dual-channel directional coupler formed by HSW on the SOI platform can be precisely controlled. The PER for quasi-TE (TM) mode is 20.49 (17.36) dB respectively with IL < 1 dB and a coupling length of 19 μm.
It should benoted that the structure's dimensions will vary ccording to the variation of the wavelength.

Acknowledgment
The authors ould like to express their gratitude to Dr. FarooqA. Khaleel for his constructive and valuable comments.

Table (2): A comparison between the design and other structures mentioned in literature.

References	λ(nm)	PER (dB)	IL(dB)	Lc(μm)	B.W(nm)	Fabrication tolerance(nm)	Simulation /experimental work
[8]	1550	31.56 (TE) 24.61(TM)	0.4 (TE) 16.2 (TM)	16	>40	$w = 20$	simulation
[9]	1550	16.8(TE) 14.1(TM)	---	15	C+L bands		Simulation+ experimental
[11]	1550	---	0.55 (TE) 0.92 (TM)	4.05	44	$w_g = \pm 150$	simulation
[14]	1550	25.5 (TE) 23.6 (TM)	<0.2	13.2	100	$w = \pm 10$	simulation
[27]	1550	30 (TE) 40 (TM)	-0.17(TE) -0.22(TM)	11	175	$w_g = \pm 30$ $L_c = \pm 350$	simulation+ experimental
Our work	700	>15 TE and TM	<1	19	7	$w = 2$ $L_c = 2000$	simulation

References:

[1] W. Jiang, X. Sun, and B. M. A. Rahman, "Compact and fabrication-tolerant polarization splitter based on horizontal triple-slot waveguide", 56, 8 (2017).

[2] D. Wang, Y. Hu, Y. Zeng, W. Wang, Y. Cai, Z. Tu, W. Yue, Q. Fang, and M. Yu, " Compact polarization beam splitter based on a 3-waveguide directional coupler with broad bandwidth performance", 2019 IEEE 16th International Conference on Group IV Photonics (GFP), (2019).

[3] C.-C. Huang, "Numerical investigations of an ultra-compact polarization beam splitter based on augmented low index guiding and subwavelength grating structures", **8**, 17338 (2018)

[4] L. Xu, Y. Wang, A. Kumar, D. Patel, E. El-Fiky, Z. Xing, R. Li, and D. V. Plant, "Polarization Beam Splitter Based on MMI Coupler With SWG Birefringence Engineering on SOI", IEEE PHOTONICS TECHNOLOGY LETTERS, **30**, 4 (2018).

[5] Z. Lin, K. Chen, Q. Huang, S. He, "Ultra Broadband Polarization Beam SplitterBased on Cascaded Mach-Zehnder Interferometers Assisted by EffectivelyAnisotropic Structures", IEEE Photonics Journal, **13**, 1 (2021).

[6] S. Mao, L. Cheng, C. Zhao, And H. Y. Fu, "Ultra-broadband and ultra-compact polarization beam splitter based on a tapered subwavelength-grating waveguide and slot waveguide", Optics Express, **29**, 18 (2021).

[7] Z. Cheng, J. Wang, Y. Huang, X. Ren, "Realization of a compact broadband polarization beam splitter using the three-waveguide coupler", IEEE Photonics Technology Letters, **31**, 22 (2019).

[8] Y. Liu, L. Chang, Z. Li, L. Liu, H. Guan and Z. Li, "Polarization beam splitter based on a silicon nitride–silica–silicon horizontal slot waveguide", Optics Letters, **44**, 6 (2019).

[9] H. Zhang, Y. Huang, S. Das, C. Li, M. Yu, P. Guo-Qiang Lo, M. Hong, and J. Thong, "Polarization splitter using horizontal slot Waveguide", OPTICS EXPRESS, **21**, 3 (2013).

[10] D. Dai, Z. Wang, J. Peters, J. E. Bowers," Compact Polarization Beam Splitter Using an Asymmetrical Mach–Zehnder Interferometer Based on Silicon-on-Insulator Waveguides", IEEE PHOTONICS TECHNOLOGY LETTERS, **24**, 8 (2012).

[11] J. Chen, D. Gao, "Ultra-compact beam splitter based on hybrid slot waveguides enhanced by silicon nitride ALIG structure", Optik, **220**, 165131 (2020).

[12] N. Zhao, C. Qiu, Y. He, Y. Zhang, Y. Su, "Broadband Polarization Beam Splitter by Using Cascaded Tapered Bent Directional Couplers", IEEE photonics journal, **11**, 4 (2019).

[13] C. Niu, Z. Liu, X. Li, X. Liu, F. Wan, J. Zheng, "High Extinction Ratio Polarization Beam Splitter Realized by Separately Coupling", IEEE PHOTONICS TECHNOLOGY LETTERS, **32**,18 (2020).

[14] J. Wang, "Design of a compact polarization beam splitter for silicon-based cross-slot waveguides", JOURNAL OF MODERN OPTICS, **67**, 15 (2020).

[15] E. Kempf, P. R. Romeo, A. Gassenq, A. Taute, P. Chantraine, J. John, A. Belarouci, S. Monfray, F. Boeuf, P. G.Charette And R. Orobtchouk, "SiN half-etch horizontal slot waveguides for integrated photonics: numerical modeling, fabrication, and characterization of passive components", Optics Express, **30**, 3 (2022).

[16] T. Huang, Y. Xie, Y. Wu, Z. Cheng, S. Zeng, and P. S. Ping, "Compact polarization beam splitter assisted by subwavelength grating in triple-waveguide directional coupler", Applied Optics, **58**, 9 (2019).

[17] J. Feng, R. Akimoto, and H. Zeng, "Asymmetric Silicon Slot-Waveguide-Assisted Polarizing Beam Splitter", IEEE Photonics Technology Letters, **28**, 12 (2016).

[18] Y. Huang, S. Zhu, H. Zhang, T.-Y. Liow, and G.-Q. Lo, "CMOS compatible horizontal nanoplasmonic slot waveguides TE-pass polarizer on silicon-on-insulator platform", OPTICS EXPRESS, **21**, 10 (2013).

[19] R. Katsumi, Y. Ota, Alto Osada, T. Yamaguchi, T. Tajiri, M. Kakuda, S.Iwamoto, H. Akiyama, and Y. Arakawa, "Quantum-dot single-photon source on a CMOS silicon photonic chip integrated using transfer printing ", APL Photonics, **4**, 036105 (2019).
[20] Farooq Abdulghafoor Khaleel, Shelan Khasro Tawfeeq, On the use of Aluminium as a plasmonic material in polarization rotators based on a hybrid plasmonic waveguide, Iraqi Journal of Laser Laser, 20, 2 (2021).
[21] L. Kong, Z. Li, Congxiu Li, L. Cao, Z.Xing, J. Cao, Y. Wang, X. Cai, And X. Zhou, "Photonic integrated quantum key distribution receiver for multiple users", Optics Express, **28**,12,(2020).
[22] J.-S. Choe, B.-S. Choi, H. Ko, and C. J. Youn, "Silica PLC-based Polarization Beam Splitter for 780 nm Free-Space Quantum Key Distribution Applications", Asia Communications and Photonics Conferene, (2016).
[23] J. -S. Choe, H. Ko, B. -S. Choi, K. -J. Kim, and C. J. Youn, "Integrated Polarization Beam Splitter Module for Polarization-Encoded Free-Space BB84 QKD", 2018 Optical Fiber Communications Conference and Exposition (OFC), (2018)
[24] T. Sneh, A. Hattori, M. Notaros, S. Corsetti, and J. Notaros, "Design of Integrated Visible-Light Polarization Rotators and Splitters", Frontiers in Optics + Laser Science (FiO/LS), (2022).
[25] Y.-F. Ma, M.-J. Sung, and D.-W. Huang, "Controlling the polarization dependence of dual-channel directional couplers formed by silicon-on-insulator slot waveguides", APPLIED OPTICS, **49**, 36 (2010).
[26] N.-C. Cheng, Y.-F. Ma, P.-H. Fu, C.-C. Chin,3 and D.-W. Huang," Horizontal slot waveguides for polarization branching control", APPLIED OPTICS, **54**, 3 (2015).
[27] Y. Tian, J. Qiu, C. Liu, S. Tian, Z.Huang, and J. Wu, "Compact polarization beam splitter with a high extinction ratio over S + C + L band", OPTICS EXPRESS, **27**, 2 (2019).

دراسة اداء مقسم استقطاب الشعاع المستند على الفتحة الافقية الذي يعمل ضمن نطاق الطول الموجي المرئي

سلوى مروان صالح، شيلان خسرو توفيق

معهد الليزر للدراسات العليا / جامعة بغداد

تعد موجهات الموجات المتكاملة لتقسيم حزمة الاستقطاب من المكونات الرئيسية في مستقبل أنظمة توزيع المفتاح الكمي. تتمثل وظيفتها في تحليل استقطاب الضوء وفصل الاستقطاب الكهربائي العرضي (TE) والاستقطاب المغناطيسي العرضي (TM) إلى موجهات مختلفة. في هذه المقالة ، تم التحقق من اداء مقسم استقطاب الشعاع المستند على الفتحة الافقية الذي يعمل بالطول الموجي 700 نانومتر. يُظهر مقسم استقطاب الشعاع المستند على الفتحة الأفقية نسبة اخماد للاستقطاب لشبه TE وللاستقطاب لشبه TM أكبر من 15 ديسيبل مع خسارة إدخال أقل من 1 ديسيبل وعرض نطاق يبلغ 7 نانومتر تقريبًا. كما تم تحليل نسبة الخطأ في التصنيع للتركيب المصمم.